

pubs.acs.org/JPCC Article

Exploring the Stability of Single-Atom Catalysts Using the Density Functional Theory-Based Global Optimization Method: H₂ Formation on VO_x/γ -Al₂O₃(100)

Ming-Hsien Lee,* Jiayan Xu, and Wenbo Xie



Cite This: J. Phys. Chem. C 2022, 126, 6973-6981



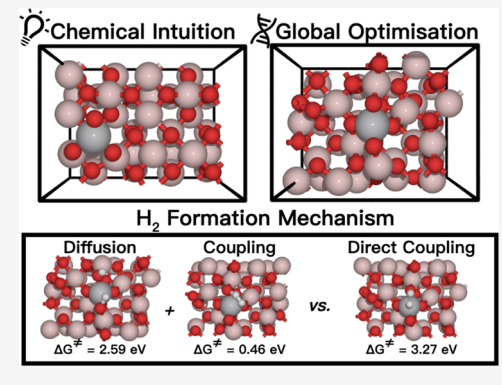
ACCESS I

Metrics & More

Article Recommendations

Supporting Information

ABSTRACT: Single-atom catalysis is indisputably one of the most trending topics in heterogeneous catalysis with distinctive performances in many important chemical reactions. However, surface reconstruction during loading of single-atom targets and its impact on vital reaction steps have rarely been studied. Herein, taking H₂ formation, a key step of alkane dehydrogenation, as an example, with genetic algorithm structure search, we reveal the structure-reactivity relationship in the H₂ formation on VO_x/γ -Al₂O₃(100). We explore a large number of VO_x/γ - $Al_2O_3(100)$ (x = 0, 1, 2, 3) structures and discover a few reconstructed structures with low formation energies. Since the pristine γ -Al₂O₃(100) support is highly stable, the production of such structures was completely induced by VO_x loading. One VO_3/γ -Al₂O₃(100) structure generates a stable VO_4 motif by reconstructing the support surface. Its distinct local chemical environment of vanadium can not only resist the oxygen removal under reductive conditions but can also offer a low-



barrier surface reaction channel to H2 formation. Moreover, the hydrogen atom prefers to diffuse into the vanadium site and then couple with another hydrogen instead of direct coupling if the initial state involves two hydrogen atoms both on oxygen sites. Therefore, the H₂ formation prefers a surface process that occurs on the vanadium—oxygen pair.

1. INTRODUCTION

Light olefins are significant compounds in the petrochemical industry, which are the feedstock to produce high-value chemicals such as polymers and oxygenates. 1,2 Alkane dehydrogenation is an effective supplement to the unprecedented growing global demands for light olefins. In general, the entire dehydrogenation pathway can be divided into two parts: the C–H bond rupture and the surface hydrogen combination. For C-H activation on transition-metal oxides, reactive sites are the acid-base pairs formed by surface metal and oxygen ions. Various mechanisms have been proposed for alkane dehydrogenation on metal oxides.3,4 Irrespective of the mechanism the dehydrogenation undergoes, it would leave hydrogen atoms on reactive sites. These hydrogen atoms would form H₂ under nonoxidative conditions; otherwise, they will block reactive sites and deactivate the catalyst. The C-H activation barrier usually in the range of 1.00-2.00 eV can be readily overcome under reaction conditions (over 500 °C and atmospheric pressure). On the other hand, the H-H formation may have a very large barrier,5 which becomes the rate-determining step. However, most studies focused on tailoring the catalytic sites for better C-H activation and neglected the H-H coupling procedure, which leaves the H₂ formation mechanism incomprehensible. It is worth mentioning that surface H is a very common surface species in many catalytic processes. $^{6-9}$ Therefore, the investigation on H_2 formation must be thoroughly carried out and the obtained insights will further facilitate the rational catalyst design for plenty of H₂-involving catalytic processes such as syngas conversion and CO₂ utilization. 10

To understand the H₂ formation in alkane dehydrogenation, it is also necessary to construct the appropriate catalyst structure under reaction conditions. Although Pt- and CrO_xbased catalysts have been successfully utilized in industrial dehydrogenation processes, they are either too expensive for commercial purposes or unable to satisfy modern environmental requirements. Recently, single-atom catalysts have received much attention due to their distinctive performance. 11-13 One experimental study demonstrated that monomeric vanadium oxide has high stability and activity in nonoxidative propane dehydrogenation (PDH).¹⁴ Vanadium oxides are usually loaded on metal oxide supports, among which Al₂O₃-based ones are the most commercially utilized. 15-21 Therefore, it is highly necessary to understand the H₂ formation on alumina-supported monomeric vanadium

Received: December 21, 2021 Revised: March 23, 2022 Published: April 15, 2022





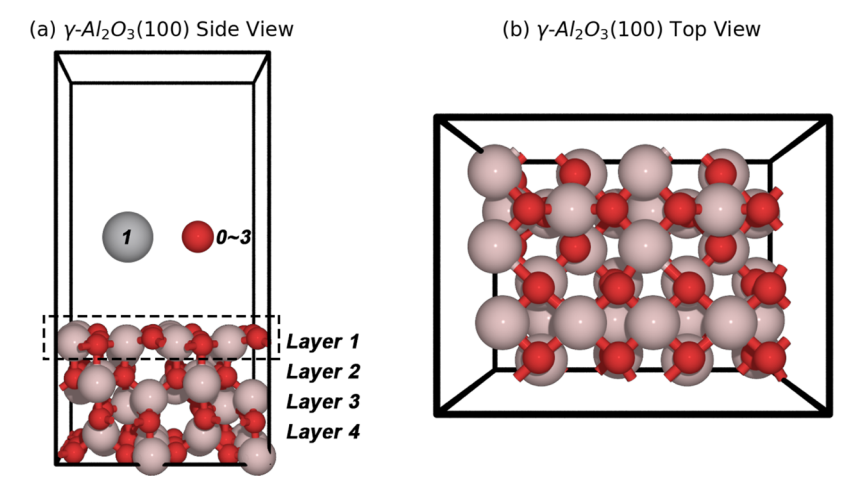


Figure 1. Side view and top view of the γ -Al₂O₃(100) model are illustrated in (a) and (b), respectively. The genetic algorithm explored the configuration of VO_x (x = 0, 1, 2, 3) with the first atomic layer shown in the dashed rectangle. The second layer can be relaxed while the third and the fourth layer are frozen during the optimization.

oxides, which is the first reason for our current work. In most computational studies, the structure models were built based on chemical intuitions. Though many exploration strategies have been proposed for bulk materials, 22,23 most surfaces used in the reaction investigation in the literature are simple ideal models. More specifically, for the current system of VO_x/γ - $Al_2O_3(100)$, one vanadium atom with some oxygen atoms was typically placed on the high symmetry sites of an ordered oxide surface to represent real catalysts. It is highly possible that the adopted structure model is not the most stable one due to the structural complexity of transition-metal oxides. Moreover, the low-energy metastable ensemble (LEME) may be missed, which can be crucial to the catalytic activity. ^{24,25} This inspired us to explore a general approach to examine a large number of VO_x/γ -Al₂O₃(100) (x = 0, 1, 2, 3) structures, which is the second reason for our work. In addition, the detailed mechanism of H₂ formation on many catalysts, particularly on oxides, remains elusive. For determining the favored mechanism for such a common reaction is highly desirable, which is the third reason for our work. In this study, we first used a density functional theory (DFT)-based global optimization method to determine stable structures of VO_x/ γ -Al₂O₃(100). Then, the favored H₂ formation mechanism on the catalyst structures we discovered was established.

2. COMPUTATIONAL METHODS

In this work, all structure stability and reaction calculations were performed using the Vienna ab initio simulation package (VASP) in the framework of spin-polarized DFT. 26,27 The exchange—correlation interaction was described by the Perdew—Burke—Ernzerhof (PBE) 28 functional. The projector augmented wave (PAW) 29 pseudopotential with a cutoff energy of 400 eV was adopted for core electrons. Additionally, the DFT + U method was applied to 3d orbitals of V with an effective $U_{\rm eff}$ of 3.2 eV to correct the on-site Coulomb interactions. To account for the van der Waals interactions, we added D3-correction to reaction calculations. However, no significant difference was observed. Therefore, we adopted PBE + U results for analysis and discussion. The detailed PBE + D3 results can be found in Table S2 in the Supporting Information.

Although the exact γ -Al₂O₃ structure is still under debate, ^{33–36} we adopted Digne's model verified by previous theoretical and experimental studies. ^{37–39} Figure 1 shows the $p(1\times2)$ γ -Al₂O₃(100) model and the substrate where VO_x (x=0,1,2,3) was added to the top Al₂O₃ layer including 10 Al and 12 O. The low-index (100) surface of γ -Al₂O₃ was chosen since it occupies 22% of the surface area and has been used in various dehydrogenation catalysts. ^{38,39} According to the size of the unit cell, Brillouin zone was sampled by a (2 × 3 × 1) Γ -centered Monkhorst–Pack mesh. ⁴⁰ The atoms in the first and the second layer are relaxed while the remaining are fixed during the structure optimization.

The global optimization procedure took advantage of the genetic algorithm (GA) structure search implemented in the atomic simulation environment (ASE), 41-45 the detailed implementation of which is described in Section 1 in the Supporting Information (SI). We first carried out coarse DFT calculations to explore the structures while the final candidates are refined with the setting listed above, which is a common strategy to speed up the search procedure. 42,43,46 In coarse calculations, the non-spin-polarized DFT without on-site Coulomb correction was utilized and the cutoff energy of the pseudopotential was reduced to 300 eV. The population size for each generation is 20 and at least 15 generations are produced to determine the global minimum of each composition. The coarse-to-accurate workflow and the choice of the population size and the generation number are shown to be effective in this work, and are described in detail in the SI

To assess the stability of various VO_x/γ -Al₂O₃(100), we use the Gibbs free energy as

$$\Delta G_{\text{VO}_x}^{\text{f}} = E_{\text{VO}_x/\gamma - \text{Al}_2\text{O}_3(100)}^{\text{tot}} - \frac{n}{2} E_{\text{V}_{\text{BCC}}}^{\text{tot}} - E_{\gamma - \text{Al}_2\text{O}_3(100)}^{\text{tot}} - m\mu_{\text{O}}$$
(1)

where the first three items are the total energy of solid compounds and the last term is the chemical potential of oxygen under the given conditions. There is no DFT + U applied to body-centered cubic (BCC) bulk vanadium. According to the experimental results, the catalyst is reoxidized using air at a bed temperature of 823 K. Therefore, we assumed that the catalyst is in equilibrium with the oxygen

Population of VO_x/γ -Al₂O₃(100)

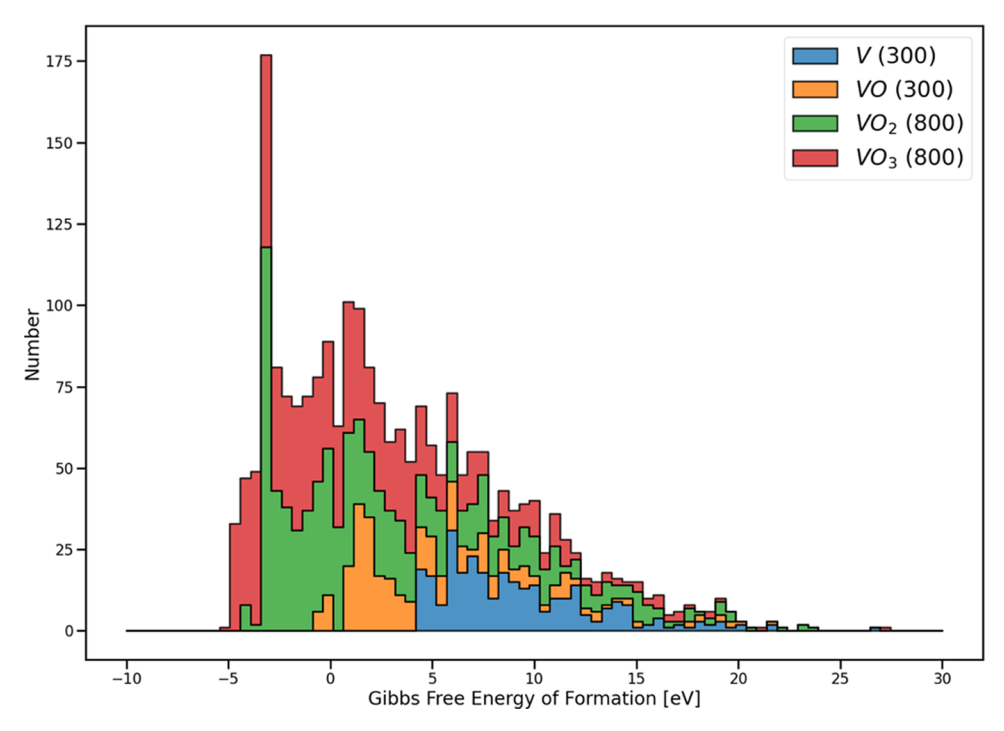


Figure 2. Illustration of the formation energies of structures explored during the GA structure search. The values in parentheses are the number of structures explored in the system. The total energy calculations adopted a relatively coarse setting that speeds up the search procedure and then the final candidates were refined by standard DFT calculations. Though there exists a total energy shift between coarse and accurate calculations, little effect was found on the relative energy order. γ -Al₂O₃(100) surfaces with VO₂ and VO₃ are generally more stable.

reservoir.⁵ The chemical potential of surface oxygen can then be estimated as

$$\begin{split} \mu_{\rm O}(T,\,p_{\rm O_2}) &= \frac{1}{2}\mu_{\rm O_2} \\ &= \frac{1}{2} \bigg(E_{\rm O_2}^{\rm tot} + E_{\rm O_2}^{\rm zpe} + \Delta H(T) + T\Delta S + k_{\rm B}T \\ &\ln \frac{p_{\rm O_2}}{p^{\theta}} \bigg) \end{split} \tag{2}$$

the formation energy serves as an indicator to show whether a structure can exist under the reaction conditions. In addition, the higher the formation energy is, the less stable the structure is.

Based on the Gibbs free energy of formation, we can utilize the Boltzmann statistics to estimate the probability of a minimum to be populated p_i as

$$p_{i} = e_{i}^{-\beta\Delta G_{i}^{f}} / \sum_{i} e^{-\beta\Delta G_{i}^{f}}$$
(3)

where ΔG_i is the formation energy difference between the given structure and the global minimum. The structure ensemble considered is made up of ones with negative Gibbs free energy of formation. To measure the reaction contributions from different structures, we adopted the weighted reaction rate of site $k_{\rm s}^{\rm w}$ proposed by Sun et al.,²⁴ which combines stability based on structure population p_i and activity by the Arrhenius equation. The definition is given by

$$k_{\rm s}^{\rm w} = A \, \exp(-\beta \Delta G_{\rm a}) p_{i} \tag{4}$$

where A is the rate constant of any reaction and ΔG_a is the free energy barrier. We assumed that the rate constant of the same reaction remains constant. The specific value of A was not considered since we aim to evaluate the relative reactivity of each structure. Furthermore, we define the relative reaction contribution of the ith site by

$$k_i^{\mathrm{w}} = k_i^{\mathrm{w}} / \sum_{j}^{\mathrm{S}} k_j^{\mathrm{w}} \tag{5}$$

where the nominator is the summation of the weighted reaction rate of S-reactive sites.

Constrained minimization was used to search transition states (TSs) that were further verified by vibrational frequencies. ^{47–50} To further understand the reaction process and the role of the active site, we performed bond-order and Mulliken charge analysis on critical TSs using CASTEP. ^{51,52} The exchange-correlation interaction was described by the PBE²⁸ functional. A cutoff energy of 750 eV was set on the plane wave basis set. The atomic Mulliken population used a radial cutoff of 3.0 Å.

3. RESULTS AND DISCUSSION

3.1. Stability of VO_x/ γ -Al₂O₃(100). We commenced our research by exploring alumina-supported vanadium oxides. During the GA structure search, there are in total 2200 VO_x/ γ -Al₂O₃(100) structures calculated using a coarse DFT setting, the formation energies of which are depicted in Figure 2.

The population of formation energies indicates that most of the structures with negative formation energy are found in VO₂ and VO₃ systems. Though there were some VO structures with negative formation energy, it turns out to be positive when

using accurate DFT calculations. Since vanadium is tetracoordinated in its common oxide V_2O_5 , it is expected that forming more V–O bonds can better stabilize the loaded vanadium. If more oxygen atoms are included in the system, it is much easier to form high-coordinated vanadium without drastically reconstructing the surface structure. Figure 3 depicts the

Ordered VO_x/γ -Al₂O₃(100)

(a) $\gamma - Al_2O_3(100)$ (b) $VO_3/\gamma - Al_2O_3(100)$ $\Delta G_f = -0.79 \text{ eV}$ (c) $V^{III}O_2/\gamma - Al_2O_3(100)$ (d) $V^{IV}O_2/\gamma - Al_2O_3(100)$ $\Delta G_f = -0.13 \text{ eV}$ $\Delta G_f = -1.35 \text{ eV}$

(e) $VO/\gamma - Al_2O_3(100)$ (f) $V/\gamma - Al_2O_3(100)$ $\Delta G_f = 0.72 \text{ eV}$ $\Delta G_f = 4.32 \text{ eV}$

Figure 3. Pristine $p(2 \times 1) \gamma$ -Al₂O₃(100) and five ordered VO_x/ γ -Al₂O₃(100) structures are depicted in (a)—(f), respectively. O is red, Al is pink, and V is gray. This notation is used throughout the paper. The formation energy becomes larger with fewer oxygen atoms. Among these five structures, VO₃/ γ -Al₂O₃(100) and V^{IV}O₂/ γ -Al₂O₃(100) are relatively more stable due to their tetracoordinated vanadium. The superscript V denotes the coordination number of the center atom.

pristine $p(2 \times 1) \gamma$ -Al₂O₃(100) and five ordered VO_x/ γ -Al₂O₃(100) structures with low formation energies. For simplicity, we leave the support formula out and use only the VO_x composition to refer to various structures. The superscript of chemical symbol denotes the coordination number of the center atom.

There are two kinds of aluminum atoms (AI^{Va} and AI^{Vb}) and oxygen atoms (O^{IIIa} and O^{IIIb}) on pristine γ - $Al_2O_3(100)$ as shown in Figure 3a, where a and b in the superscript are used to mark two different sites. Our results show that to stabilize the structure, vanadium should coordinate with as many oxygen atoms as possible. Thus, the suitable loading place is the acid—base pair formed by AI^{Va} and O^{IIIa} . The structure of VO_3 in Figure 3b has the lowest formation energy of -0.79 eV due to its stable tetracoordinated vanadium. There are two ordered VO_2 structures distinguished by the coordination

number of vanadium, as shown in Figure 3c,d. The first one has three-coordinated vanadium with a larger formation energy of -0.13 eV (the larger formation energy means that the structure is less stable, as mentioned above). This structure was used in a recent study. The second one located in our work is substantially more stable than the one reported in the literature since it forms the fourth V–O bond by breaking the AlVb–O bond, which lowers the formation energy by 1.22 eV. For the VO structure in Figure 3e, vanadium can only form three V–O bonds, which largely increases the formation energy to 0.72 eV. The single vanadium-loaded structure in Figure 3f has a formation energy of 4.32 eV and is highly unstable compared to those monomeric vanadium oxides.

In addition to the ordered structures, GA search also produced a few disordered structures that reconstruct the γ -Al₂O₃(100) surface. To check whether the reconstruction is due to the nature of γ -Al₂O₃(100), we used GA to explore possible reconstructions of the γ -Al₂O₃(100) surface as well, but no reconstruction was found. The histogram of formation energies is shown in Figure S3 in the SI. This indicates that the surface reconstruction is completely induced by the VO_x loading. For structures with single vanadium loading, we found that monomeric vanadium oxides are prone to remain on the top of the γ -Al₂O₃(100) surface instead of being the bulk dopant (see Figure S4 in the SI). The most stable structure such as the one shown in Figure S5 in the SI, is that in which the vanadium substitutes the lattice aluminum to form five V-O bonds. This reconstruction stabilizes the vanadium atom but pushes the aluminum atom to diffuse to the surface and become less coordinated, which lowers the formation energy of 0.18 eV compared to the manually constructed one. With VO and VO2 structures, vanadium can form relatively stable VO₃ and VO₄ motifs without modifying the γ -Al₂O₃(100) lattice. Although some disordered structures are discovered, the most stable structure is still the ordered surface with VO or V^{IV}O₂ (the superscript indicates that vanadium is tetracoordinated). Interestingly, among VO₃ structures, we find that there are two disordered structures lower in energy by 0.28 and 0.38 eV compared to the ordered one. Furthermore, the strong reductive atmosphere in PDH may remove low-coordinated oxygen atoms around the vanadium site.⁵ Figure 4 shows three VO₃ structures with their possible reduction pathways, which include one manually constructed structure and two disordered structures that are discovered in the GA search. The two significantly disordered structures are denoted as VO₃ ms (superscript ms means metastable) in Figure 4a and VO3s (superscript s means stable) in Figure 4b. The reduction in the energy profile is shown in Figure 4c. For consecutively removing two oxygen atoms on the ordered VO₃ changes the formation energies by 0.66 and 2.07 eV, respectively. The corresponding reduced structure is shown in Figure 3. This reduction pathway indicates that the first removal is relatively easier and further reduction becomes much more difficult. It is noteworthy that the generated VIIIO2 after the first oxygen removal will transform into a more stable structure VIVO2. We also studied the reduction of disordered VO₃ structures. These two disordered VO₃ structures both have one-dimensional Al^{IV}-AlIV-VIV wire on the surface, which produce a distinct local chemical environment. The metastable one VO3 ms generates a VO₄ motif without floating the V=O bond, which indicates that it may resist the reduction atmosphere. The removal of oxygen from the VO₄ motif requires a large energy of 2.05 eV

Surface VO_x Reduction Pathway

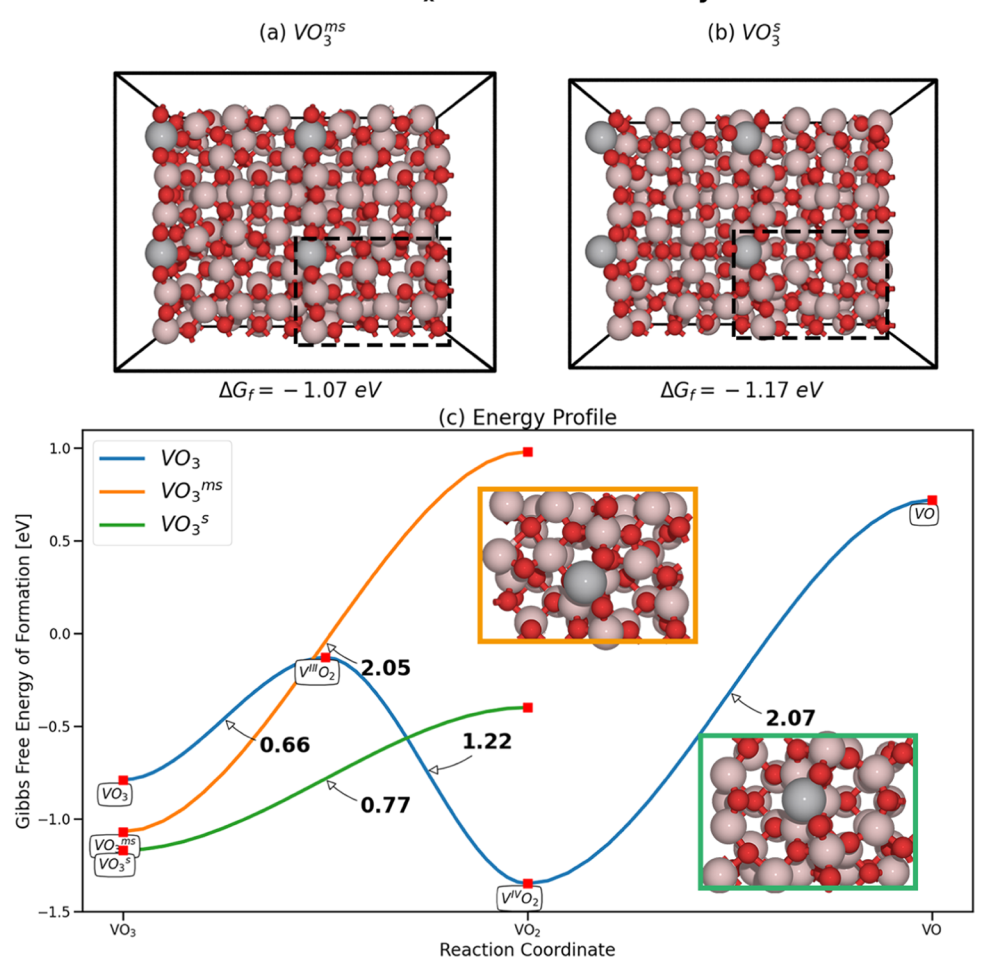


Figure 4. Two disordered structures, VO_3^{ms} (the superscript ms denotes metastable) and VO_3^{s} (the superscript s denotes stable), are illustrated in (a) and (b), respectively, both of which generate stable VO_4 motifs. The structural difference between these two disordered structures is that VO_3^{s} has one V=O bond while VO_3^{ms} does not. The reduction pathways of VO_3 -variants are exhibited in (c). The reduced VO_3^{ms} structure is depicted in the orange box while the reduced VO_3^{s} is in the green box. VO_3^{ms} requires more energy to remove the first oxygen compared to VO_3^{s} which indicates that it is more stable under reductive conditions.

due to the cleavage of one V–O bond and one Al–O bond, which would create a thermodynamically unfavorable structure (with positive formation energy). The most stable one, VO $_3$ s, also creates a VO $_4$ motif but with one floating V=O bond that is similar to V^{IV}O $_2$ and VO $_3$. The removal of such an oxygen atom requires only 0.77 eV that is close to the one for VO $_3$, which generates a reduced structure with a formation energy of –0.40 eV. Since it has a lower formation energy compared to the ordered VO $_3$ and much higher reduction energy than the other two VO $_3$ structures, VO $_3$ s can be considered as one of the structures under the reaction condition. The structure ensemble under the reaction conditions consists of three structures with considerable negative formation energy, namely VO $_2$, VO $_3$ s, and VO $_3$ s, the Boltzmann populations of which are 91, 7.2, and 1.8%, respectively.

3.2. H₂ **Formation Mechanism.** Having thoroughly determined the stable structures and analyzed the geometric characteristics of low-energy structures, we were in the solid position to investigate the H₂ formation reaction mechanism on ordered structures as well as on disordered VO₃-variants. This reaction involves two adsorbed hydrogen atoms to form hydrogen gas molecules. The reactive acid—base pair is the vanadium atom and the neighboring two-coordinated oxygen

atom. Although H can adsorb on the three-coordinated oxygen, the H-H coupling would introduce a large distortion in the local structure where the V-O bond cleavage occurs. In other words, the reaction barrier can be very large. Therefore, we first considered the reactions starting with one H on vanadium and another on two-coordinated oxygen. The TS of H₂ formation was located and the resulting reaction energies and geometric variables in the TSs are listed in Table 1 while the corresponding structures can be found in Figure S6 in the SI. The free energies were computed with correction by harmonic-limit approximation at 550 °C and 1 atm. We also located the TSs with one partially-activated H₂ molecule over the O site, which has been found in a recent study (see Figure S7 in the SI). This is also the only type of TS we located on ordered VO₃. However, the distance between the upper H and the vanadium site is usually very large (over 3.0 Å). Thus, this kind of TS cannot be considered as the one for the surface H-H coupling. For the bond distances in the TSs, the typical H-H bond distance in the TS is ca. 1.00 Å that is a little longer than the bond distance of 0.75 Å in the H₂ molecule, which is reasonable. The H-V bond distances are around 1.8 Å except for the TS of the one on VO. The longer H-V distance of 1.92 Å can be attributed to the low valence state of the vanadium

Table 1. H_2 Formation on Various Sites, Where ΔG_a is the Activation Free Energy Barrier and ΔG_r is the Reaction Free Energy Change^a

surface	site	$rac{\Delta G_{ m a}}{ m [eV]}$	$rac{\Delta G_{ m r}}{[{ m eV}]}$	$\begin{bmatrix} d_{\rm H-H} \\ {\rm [A]} \end{bmatrix}$	$^{d_{\rm H-O}}_{\rm [A]}$	$^{d_{\rm H-V}}_{\rm [A]}$
VO	$O^{II}-V$	0.56	-1.15	1.04	1.27	1.92
$V^{III}O_2$	$O^{II}-V$	1.13	-0.81	0.995	1.32	1.86
$V^{IV}O_2$	O^{II} $-V$	0.75	-1.32	1.00	1.34	1.84
VO_3^{ms} -1	O^{II} $-V$	0.46	-2.91	1.04	1.23	1.81
VO_3^{ms} -2	$O^{II}-V$	0.54	-3.14	1.07	1.14	1.85
VO_3^s -1	$O^{I}-V$	0.80	-2.13	1.00	1.25	1.82
VO_3^s-2	$O^{II}-V$	0.64	-2.28	1.06	1.23	1.84
VO_3^s-3	$O^{II}-V$	0.66	-2.27	1.00	1.26	1.82

^aThree critical interatomic distances in the transition states are listed as $d_{\rm H-H}$, $d_{\rm H-O}$, and $d_{\rm H-V}$.

which is coordinated by fewer oxygen atoms. The H–O bond distances have a relatively larger range from 1.00 to 1.35 Å. For the reaction energies, the reaction becomes more thermodynamically favorable with more oxygen atoms. On the other hand, there is no obvious relation between the reaction barrier and the number of oxygen atoms in the added VO_x . Among all the reactive sites, the reaction on the metastable structure VO_3^{ms} has the lowest barrier of 0.46 eV (VO_3^{ms} -1) that is lower than half of the one on $V^{III}O_2$ (1.13 eV). In tandem with its resistance to oxygen removal, VO_3^{ms} may be the reactive site

responsible for $\rm H_2$ formation during the PDH process. When considering the reactive structure ensemble constructed in Section 3.1 and the reactive site with the lowest barrier, the weighted reaction rate analysis shows that the rate contributions from $\rm VO_2$, $\rm VO_3^s$, and $\rm VO_3^{ms}$ are 39.6, 14.8, and 45.6%, respectively. It is noteworthy that $\rm VO_3^{ms}$ contributes almost half of the rate with only 1.7% population. This observation further demonstrates that the minority structure can be crucial to the activity.

Since vanadium is the site for C-H activation, 5,18-20 it is highly possible that the configuration after the second H abstraction of alkane has two hydrogen atoms, both adsorbed on the oxygen sites. Taking H₂ formation on VO₃^{ms} as an example, we examined the diffusion pathways for H moving to the nearby vanadium atom. The corresponding TSs were located and the entire reaction pathway and the TS structures are shown in Figure 5. The active site made up of three atoms are denoted as V, Oa, and Ob, while the reactants include two hydrogen atoms which are marked as Ha and Hb. The diffusion from Ob to V has a large energy barrier of 2.59 eV due to O-H bond breaking. Once H^b moves to adsorb on V, it can couple with Ha on the Oa site by overcoming a small barrier of 0.46 eV, as discussed above. Alternatively, H^b can directly couple with Ha, but the energy barrier of 3.27 eV is large, which is larger than the diffusion barrier by 0.68 eV. Based on the thermodynamic data, the H-H coupling mechanism prefers

H-H Coupling Mechanism on VO₃^{ms}/γ-Al₂O₃(100)

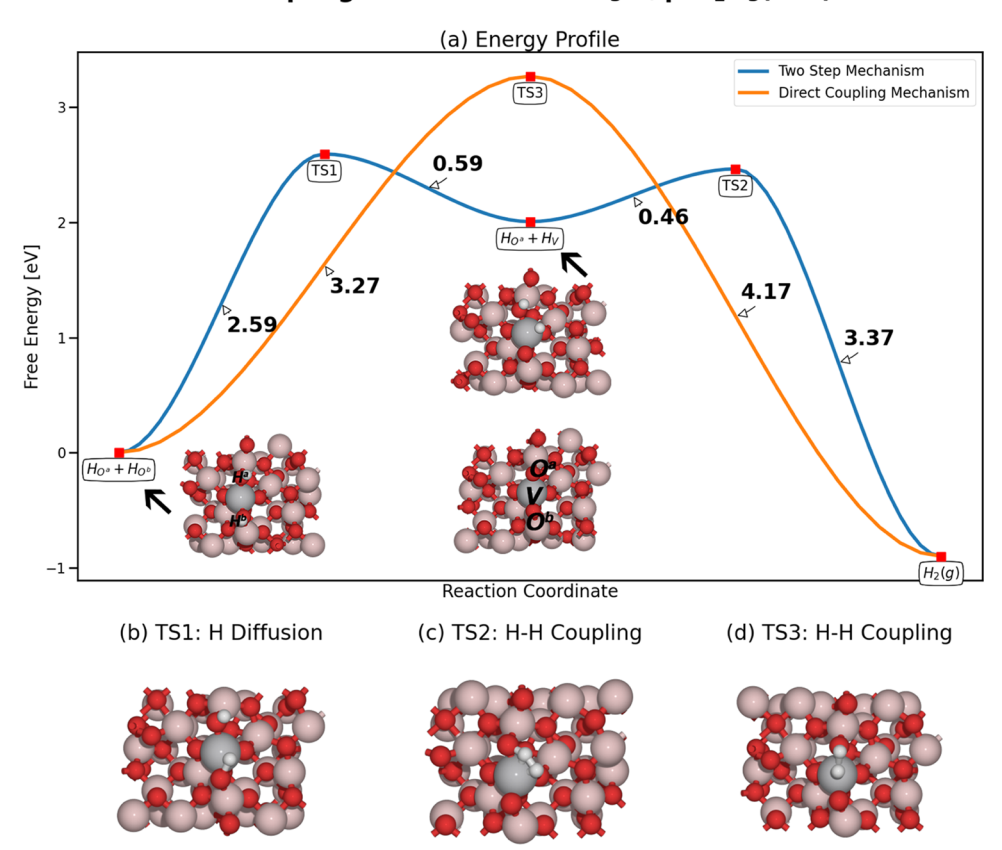


Figure 5. Two H_2 formation mechanisms, two-step mechanism and direct-coupling mechanism, with their transition states are exhibited where H is shown in white. The energy profile of the diffusion—coupling mechanism and the direct-coupling mechanism are shown in (a). The diffusion transition state and two coupling transition states are shown in (b), (c), and (d), respectively. Two hydrogen atoms are both on the adsorption sites in the diffusion—coupling mechanism, while one of them is far from the vanadium site (distance 2.32 Å) in the direct coupling.

Bond-Order and Charge Analysis

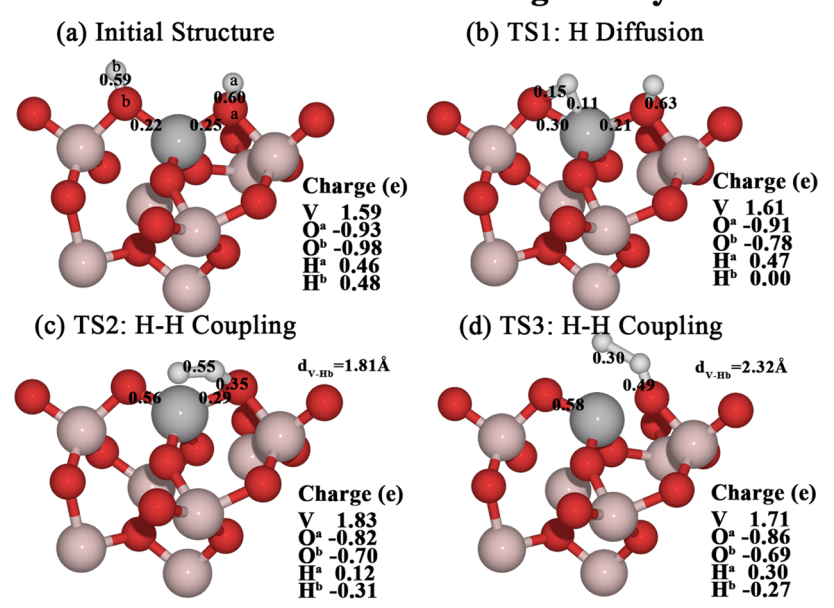


Figure 6. Bond-order and Mulliken charge analyses were performed on four critical structures in the H_2 formation mechanism. The initial structure is shown in (a) while three significant transition states are shown in (b), (c), and (d), respectively. The number marked on the bond is the bond order. The large diffusion barrier from (a) to (b) is due to the weakening of the O–H bond, which is indicated by the decrease of bond order from 0.59 to 0.15. Although there is no covalent bond between H and V as shown in (c) and (d), the strong electrostatic interaction makes H–H coupling close to the surface and stabilizes the transition state.

the diffusion-coupling pathway even if the direct coupling route exists.

We further performed bond-order and Mulliken charge analysis to understand these reaction processes and the role of vanadium. Four critical structures with bond-order values and charges marked are shown in Figure 6. This analysis focuses on the active sites and the reactants. The H2 formation mechanism starts from the initial structure with both hydrogen atoms adsorbed on oxygen sites, which has two stable O-H bonds with a bond order of around 0.60, as labeled in Figure 6a. For the H diffusion process, as shown in Figure 6b, H^b forms weak covalent bonds with the Ob and V, the bond-order values of which are 0.15 and 0.11, respectively. There is a large decrease in the Ob-Hb bond order from 0.59 to 0.15 during diffusion. This further proves that the large diffusion barrier of 2.59 eV is due to the change of the O^b-H^b bond. For the first kind of H-H coupling TS shown in Figure 6c, it is interesting that there is no covalent bond between H^b and V. Meanwhile, there are considerable net charges on these two atoms, -0.31 e for H^b and 1.83 e for V. With a small interatomic distance of 1.81 Å, the electrostatic interaction between H^b and V is strong, which stabilizes the TS and makes this reaction a surface process. The situation is very similar for the second coupling TS shown in Figure 6d. There is no covalent bond between H^b and V, which is similar to that of the first coupling TS. However, the electrostatic interaction is weaker since the distance between H^b and V is larger (2.32 Å) and the net charges on these two atoms are smaller (1.71 e on V and -0.27e on H^b). The weak electrostatic interaction in this TS may be one of the reasons for its high energy barrier. Moreover, the covalent bond between Oa and V is cleaved in the TS, which partially contributes to the high energy barrier. According to the analysis of the bond order and the Mulliken charge, we further demonstrate that the coupling mechanism prefers a surface process.

4. CONCLUSIONS

In conclusion, this work represents one of the first attempts to systematically investigate the stable structures of single-atom catalysts using the DFT-based global optimization method. We have found that loading monomeric vanadium oxide would induce the reconstruction of the γ -Al₂O₃(100) support. Among a large number of explored configurations, the VO₃ ms structure forms a stable VO₄ motif that resists oxygen removal and provides low-barrier H2 formation sites. According to the Boltzmann population and weighted reaction rate, VO₃^{ms} can contribute a large part of the total reaction rate with a small population. Furthermore, the direct-coupling mechanism beginning with both hydrogen atoms adsorbed on oxygen is thermodynamically unfavorable. The favored mechanism is that one hydrogen diffuses to vanadium and then couples with another oxygen-adsorbed hydrogen. This mechanism is further confirmed by the bond-order and Mulliken charge analysis. Based on these results, we suggest that the reasonable H₂ formation pathway should be a surface process that occurs on the vanadium-oxygen pair in contrast to the pathways reported in the literature. This resolves the problem of the H_2 formation mechanism on VO_x/γ - $Al_2O_3(100)$, which is a crucial step in PDH. This reconstruction process not only produces more stable structures but also generates a distinct local chemical environment that builds active sites. This novel discovery indicates that determining the structures of supported catalysts is not straightforward and special care must be taken during the modeling of catalyst active sites. It is necessary to explore such catalysts using global optimization methods to obtain a better understanding of the structurereactivity relationship. This would guide us to explore more single-atom catalyst systems in the future.

ASSOCIATED CONTENT

5 Supporting Information

The Supporting Information is available free of charge at https://pubs.acs.org/doi/10.1021/acs.jpcc.1c10740.

Detailed implementation of genetic algorithm search; influence of different DFT settings on structures' energy order; more discussion on the structure search of pristine γ -Al₂O₃(100) and V/ γ -Al₂O₃(100); structures of H₂ formation transition states; and influence of D3 corrections on reaction data (PDF)

AUTHOR INFORMATION

Corresponding Author

Ming-Hsien Lee — Department of Physics, Tamkang University, New Taipei City 25137, Taiwan; ⊙ orcid.org/ 0000-0003-3956-181X; Email: mhslee@mail.tku.edu.tw

Authors

Jiayan Xu — School of Chemistry and Chemical Engineering, Queen's University Belfast, Belfast BT9 SAG, U.K.; orcid.org/0000-0001-9897-5778

Wenbo Xie — School of Chemistry and Chemical Engineering, Queen's University Belfast, Belfast BT9 5AG, U.K.; orcid.org/0000-0001-5321-2494

Complete contact information is available at: https://pubs.acs.org/10.1021/acs.jpcc.1c10740

Notes

The authors declare no competing financial interest.

ACKNOWLEDGMENTS

We are grateful for use of the computing resources at the Northern Ireland High Performance Computing (NI-HPC) service funded by EPSRC (EP/T022175). J.X. acknowledges the financial support from the Queen's University Belfast and the China Scholarship Council.

REFERENCES

- (1) Sattler, J. J. H. B.; Ruiz-Martinez, J.; Santillan-Jimenez, E.; Weckhuysen, B. M. Catalytic Dehydrogenation of Light Alkanes on Metals and Metal Oxides. *Chem. Rev.* **2014**, *114*, 10613–10653.
- (2) Dai, Y.; Gao, X.; Wang, Q.; Wan, X.; Zhou, C.; Yang, Y. Recent Progress in Heterogeneous Metal and Metal Oxide Catalysts for Direct Dehydrogenation of Ethane and Propane. *Chem. Soc. Rev.* **2021**, *50*, 5590–5630.
- (3) Joubert, J.; Delbecq, F.; Sautet, P. Alkane Metathesis by a Tungsten Carbyne Complex Grafted on Gamma Alumina: Is There a Direct Chemical Role of the Support? *J. Catal.* **2007**, *251*, 507–513.
- (4) Dixit, M.; Kostetskyy, P.; Mpourmpakis, G. Structure—Activity Relationships in Alkane Dehydrogenation on γ -Al₂O₃: Site-Dependent Reactions. *ACS Catal.* **2018**, *8*, 11570–11578.
- (5) Xiong, C.; Chen, S.; Yang, P.; Zha, S.; Zhao, Z.-J.; Gong, J. Structure—Performance Relationships for Propane Dehydrogenation over Aluminum Supported Vanadium Oxide. *ACS Catal.* **2019**, *9*, 5816—5827.
- (6) Raybaud, P.; Chizallet, C.; Mager-Maury, C.; Digne, M.; Toulhoat, H.; Sautet, P. From γ -Alumina to Supported Platinum Nanoclusters in Reforming Conditions: 10 Years of DFT Modeling and Beyond. *J. Catal.* **2013**, *308*, 328–340.
- (7) Xie, W.; Xu, J.; Ding, Y.; Hu, P. Quantitative Studies of the Key Aspects in Selective Acetylene Hydrogenation on Pd(111) by Microkinetic Modeling with Coverage Effects and Molecular Dynamics. ACS Catal. 2021, 11, 4094–4106.

- (8) Xie, W.; Hu, P. Influence of Surface Defects on Activity and Selectivity: A Quantitative Study of Structure Sensitivity of Pd Catalysts for Acetylene Hydrogenation. *Catal. Sci. Technol.* **2021**, *11*, 5212–5222.
- (9) Sun, G.; Fuller, J. T.; Alexandrova, A. N.; Sautet, P. Global Activity Search Uncovers Reaction Induced Concomitant Catalyst Restructuring for Alkane Dissociation on Model Pt Catalysts. *ACS Catal.* **2021**, *11*, 1877–1885.
- (10) Jiang, X.; Nie, X.; Guo, X.; Song, C.; Chen, J. G. Recent Advances in Carbon Dioxide Hydrogenation to Methanol Via Heterogeneous Catalysis. *Chem. Rev.* **2020**, *120*, 7984–8034.
- (11) Sun, G.; Zhao, Z. J.; Mu, R.; Zha, S.; Li, L.; Chen, S.; Zang, K.; Luo, J.; Li, Z.; Purdy, S. C.; et al. Breaking the Scaling Relationship Via Thermally Stable Pt/Cu Single Atom Alloys for Catalytic Dehydrogenation. *Nat. Commun.* **2018**, *9*, No. 4454.
- (12) Nakaya, Y.; Hirayama, J.; Yamazoe, S.; Shimizu, K. I.; Furukawa, S. Single-Atom Pt in Intermetallics as an Ultrastable and Selective Catalyst for Propane Dehydrogenation. *Nat. Commun.* **2020**, *11*, No. 2838.
- (13) Hannagan, R. T.; Giannakakis, G.; Réocreux, R.; Schumann, J.; Finzel, J.; Wang, Y.; Michaelides, A.; Deshlahra, P.; Christopher, P.; Flytzani-Stephanopoulos, M.; et al. First-Principles Design of a Single-Atom—Alloy Propane Dehydrogenation Catalyst. *Science* **2021**, *372*, 1444—1447.
- (14) Zhang, T.; Guo, X.; Song, C.; Liu, Y.; Zhao, Z. Fabrication of Isolated VO_x Sites on Alumina for Highly Active and Stable Non-Oxidative Dehydrogenation. *J. Phys. Chem. C* **2021**, *125*, 19229–19237.
- (15) Fu, H.; Liu, Z.-P.; Li, Z.-H.; Wang, W.-N.; Fan, K.-N. Periodic Density Functional Theory Study of Propane Oxidative Dehydrogenation over V₂O₅(001) Surface. *J. Am. Chem. Soc.* **2006**, *128*, 11114–11123.
- (16) Carrero, C. A.; Schloegl, R.; Wachs, I. E.; Schomaecker, R. Critical Literature Review of the Kinetics for the Oxidative Dehydrogenation of Propane over Well-Defined Supported Vanadium Oxide Catalysts. *ACS Catal.* **2014**, *4*, 3357–3380.
- (17) Fu, H.; Duan, Z.; Henkelman, G. Computational Study of Structure and Reactivity of Oligomeric Vanadia Clusters Supported on Anatase and Rutile TiO₂ Surfaces. *J. Phys. Chem. C* **2015**, *119*, 15160–15167.
- (18) Liu, G.; Zhao, Z.-J.; Wu, T.; Zeng, L.; Gong, J. Nature of the Active Sites of VO_x/Al_2O_3 Catalysts for Propane Dehydrogenation. ACS Catal. 2016, 6, 5207–5214.
- (19) Zhao, Z. J.; Wu, T.; Xiong, C.; Sun, G.; Mu, R.; Zeng, L.; Gong, J. Hydroxyl-Mediated Non-Oxidative Propane Dehydrogenation over VO_x/γ -Al₂O₃ Catalysts with Improved Stability. *Angew. Chem., Int. Ed.* **2018**, *57*, 6791–6795.
- (20) Xie, Y.; Luo, R.; Sun, G.; Chen, S.; Zhao, Z. J.; Mu, R.; Gong, J. Facilitating the Reduction of V-O Bonds on VO_x/ZrO₂ Catalysts for Non-Oxidative Propane Dehydrogenation. *Chem. Sci.* **2020**, 11, 3845—3851
- (21) Shan, Y.-L.; Zhao, W.-T.; Zhao, S.-L.; Wang, X.-X.; Sun, H.-L.; Yu, W.-L.; Ding, J.-W.; Feng, X.; Chen, D. Effects of Alumina Phases on the Structure and Performance of VO_x/Al_2O_3 Catalysts in Non-Oxidative Propane Dehydrogenation. *Mol. Catal.* **2021**, *504*, No. 111466.
- (22) Yu, J.; Zhang, B.; Zhang, X.; Wang, Y.; Wu, K.; Lee, M. H. Finding Optimal Mid-Infrared Nonlinear Optical Materials in Germanates by First-Principles High-Throughput Screening and Experimental Verification. ACS Appl. Mater. Interfaces 2020, 12, 45023–45035.
- (23) Zhang, B.; Zhang, X.; Yu, J.; Wang, Y.; Wu, K.; Lee, M.-H. First-Principles High-Throughput Screening Pipeline for Nonlinear Optical Materials: Application to Borates. *Chem. Mater.* **2020**, *32*, 6772–6779.
- (24) Sun, G.; Sautet, P. Metastable Structures in Cluster Catalysis from First-Principles: Structural Ensemble in Reaction Conditions and Metastability Triggered Reactivity. *J. Am. Chem. Soc.* **2018**, *140*, 2812–2820.

- (25) Zhang, Z.; Zandkarimi, B.; Alexandrova, A. N. Ensembles of Metastable States Govern Heterogeneous Catalysis on Dynamic Interfaces. Acc. Chem. Res. 2020, 53, 447-458.
- (26) Kresse, G.; Furthmüller, J. Efficiency of Ab-Initio Total Energy Calculations for Metals and Semiconductors Using a Plane-Wave Basis Set. Comput. Mater. Sci. 1996, 6, 15-50.
- (27) Kresse, G.; Furthmüller, J. Efficient Iterative Schemes for Ab Initio Total-Energy Calculations Using a Plane-Wave Basis Set. Phys. Rev. B 1996, 54, 11169-11186.
- (28) Perdew, J. P.; Burke, K.; Ernzerhof, M. Generalized Gradient Approximation Made Simple. Phys. Rev. Lett. 1996, 77, 3865-3868.
- (29) Kresse, G.; Joubert, D. From Ultrasoft Pseudopotentials to the Projector Augmented-Wave Method. Phys. Rev. B 1999, 59, 1758-
- (30) Wang, L.; Maxisch, T.; Ceder, G. Oxidation Energies of Transition Metal Oxides within the GGA+U Framework. Phys. Rev. B 2006, 73, No. 195107.
- (31) Grimme, S.; Antony, J.; Ehrlich, S.; Krieg, H. A Consistent and Accurate Ab Initio Parametrization of Density Functional Dispersion Correction (DFT-D) for the 94 Elements H-Pu. J. Chem. Phys. 2010, 132, No. 154104.
- (32) Grimme, S.; Ehrlich, S.; Goerigk, L. Effect of the Damping Function in Dispersion Corrected Density Functional Theory. J. Comput. Chem. 2011, 32, 1456-1465.
- (33) Lee, M.-H.; Cheng, C.-F.; Heine, V.; Klinowski, J. Distribution of Tetrahedral and Octahedral Al Sites in Gamma Alumina. Chem. Phys. Lett. 1997, 265, 673-676.
- (34) Pinto, H. P.; Nieminen, R. M.; Elliott, S. D. Ab Initio Study of γ-Al₂O₃ Surfaces. Phys. Rev. B **2004**, 70, No. 125402.
- (35) Prins, R. On the Structure of Γ -Al₂o₃. *J. Catal.* **2020**, 392, 336– 346.
- (36) Lee, M.-H. Advanced Pseudopotentials for Large Scale Electronic Structure Calculations with Application to a Study of Weakly Ordered Material - Gamma-Al2O3; Cambridge University, 1995.
- (37) Krokidis, X.; Raybaud, P.; Gobichon, A.-E.; Rebours, B.; Euzen, P.; Toulhoat, H. Theoretical Study of the Dehydration Process of Boehmite to γ -Alumina. J. Phys. Chem. B **2001**, 105, 5121–5130.
- (38) Raybaud, P.; Digne, M.; Iftimie, R.; Wellens, W.; Euzen, P.; Toulhoat, H. Morphology and Surface Properties of Boehmite (γ-AlOOH): A Density Functional Theory Study. J. Catal. 2001, 201,
- (39) Digne, M.; Sautet, P.; Raybaud, P.; Euzen, P.; Toulhoat, H. Use of DFT to Achieve a Rational Understanding of Acid-Basic Properties of γ-Alumina Surface. J. Catal. 2004, 226, 54–68.
- (40) Monkhorst, H. J.; Pack, J. D. Special Points for Brillouin-Zone Integrations. Phys. Rev. B 1976, 13, 5188-5192.
- (41) Deaven, D. M.; Ho, K. M. Molecular Geometry Optimization with a Genetic Algorithm. Phys. Rev. Lett. 1995, 75, 288-291.
- (42) Vilhelmsen, L. B.; Hammer, B. Systematic Study of Au₆ to Au₁₂ Gold Clusters on MgO(100) F Centers Using Density-Functional Theory. Phys. Rev. Lett. 2012, 108, No. 126101.
- (43) Vilhelmsen, L. B.; Walton, K. S.; Sholl, D. S. Structure and Mobility of Metal Clusters in Mofs: Au, Pd, and Aupd Clusters in Mof-74. J. Am. Chem. Soc. 2012, 134, 12807-12816.
- (44) Vilhelmsen, L. B.; Hammer, B. A Genetic Algorithm for First Principles Global Structure Optimization of Supported Nano Structures. J. Chem. Phys. 2014, 141, No. 044711.
- (45) Larsen, A. H.; Mortensen, J. J.; Blomqvist, J.; Castelli, I. E.; Christensen, R.; Dulak, M.; Friis, J.; Groves, M. N.; Hammer, B.; Hargus, C.; et al. The Atomic Simulation Environment-a Python Library for Working with Atoms. J. Phys.: Condens. Matter 2017, 29,
- (46) Wu, S. Q.; Ji, M.; Wang, C. Z.; Nguyen, M. C.; Zhao, X.; Umemoto, K.; Wentzcovitch, R. M.; Ho, K. M. An Adaptive Genetic Algorithm for Crystal Structure Prediction. J. Phys.: Condens. Matter 2014, 26, No. 035402.
- (47) Alavi, A.; Hu, P.; Deutsch, T.; Silvestrelli, P. L.; Hutter, J. CO Oxidation on Pt(111): An Ab Initio Density Functional Theory Study. Phys. Rev. Lett. 1998, 80, 3650-3653.

- (48) Liu, Z.-P.; Hu, P. General Rules for Predicting Where a Catalytic Reaction Should Occur on Metal Surfaces: A Density Functional Theory Study of C-H and C-O Bond Breaking/Making on Flat, Stepped, and Kinked Metal Surfaces. J. Am. Chem. Soc. 2003, 125, 1958-1967.
- (49) Michaelides, A.; Liu, Z.-P.; Zhang, C. J.; Alavi, A.; King, D. A.; Hu, P. Identification of General Linear Relationships between Activation Energies and Enthalpy Changes for Dissociation Reactions at Surfaces. J. Am. Chem. Soc. 2003, 125, 3704-3705.
- (50) Wang, H.-F.; Liu, Z.-P. Comprehensive Mechanism and Structure-Sensitivity of Ethanol Oxidation on Platinum: New Transition-State Searching Method for Resolving the Complex Reaction Network. J. Am. Chem. Soc. 2008, 130, 10996-11004.
- (51) Payne, M. C.; Teter, M. P.; Allan, D. C.; Arias, T. A.; Joannopoulos, J. D. Iterative Minimization Techniques Forab Initiototal-Energy Calculations: Molecular Dynamics and Conjugate Gradients. Rev. Mod. Phys. 1992, 64, 1045-1097.
- (52) Clark, S. J.; Segall, M. D.; Pickard, C. J.; Hasnip, P. J.; Probert, M. I. J.; RefsonV, K.; Payne, M. C. First Principles Methods Using CASTEP. Z. Kristallogr. 2005, 220, 567-570.

□ Recommended by ACS

Computational Investigation of Hydriding and Strain **Effects on the Binding Energies of Electrochemical CO2RR and HER Intermediates**

Jongpil Ye.

MARCH 21, 2022

THE JOURNAL OF PHYSICAL CHEMISTRY C

RFAD 🗹

Mechanism of Methanol Decomposition over Single-Site Pt₁/CeO₂ Catalyst: A DRIFTS Study

Zhiyuan Qi, Gabor A. Somorjai, et al.

DECEMBER 24, 2020

JOURNAL OF THE AMERICAN CHEMICAL SOCIETY

READ **C**

Correlating the Synthesis, Structure, and Catalytic Performance of Pt-Re/TiO2 for the Aqueous-Phase Hydrogenation of Carboxylic Acid Derivatives

Moritz O. Haus, Regina Palkovits, et al.

APRIL 13, 2021 ACS CATALYSIS

READ **C**

Ethanol Electro-oxidation Reaction Selectivity on Platinum in Aqueous Media

Rubén Rizo, Juan M. Feliu, et al.

JULY 12, 2022

ACS SUSTAINABLE CHEMISTRY & ENGINEERING

READ **C**

Get More Suggestions >